Electric field gradients during electrophoretic fractionation in microfabricated post arrays

Shokoufeh Kazemlou & Neda Nazemifard

Microfluidics and Nanofluidics

ISSN 1613-4982
Volume 17
Number 6

Microfluid Nanofluid (2014) 17:993-1002
DOI 10.1007/s10404-014-1392-0

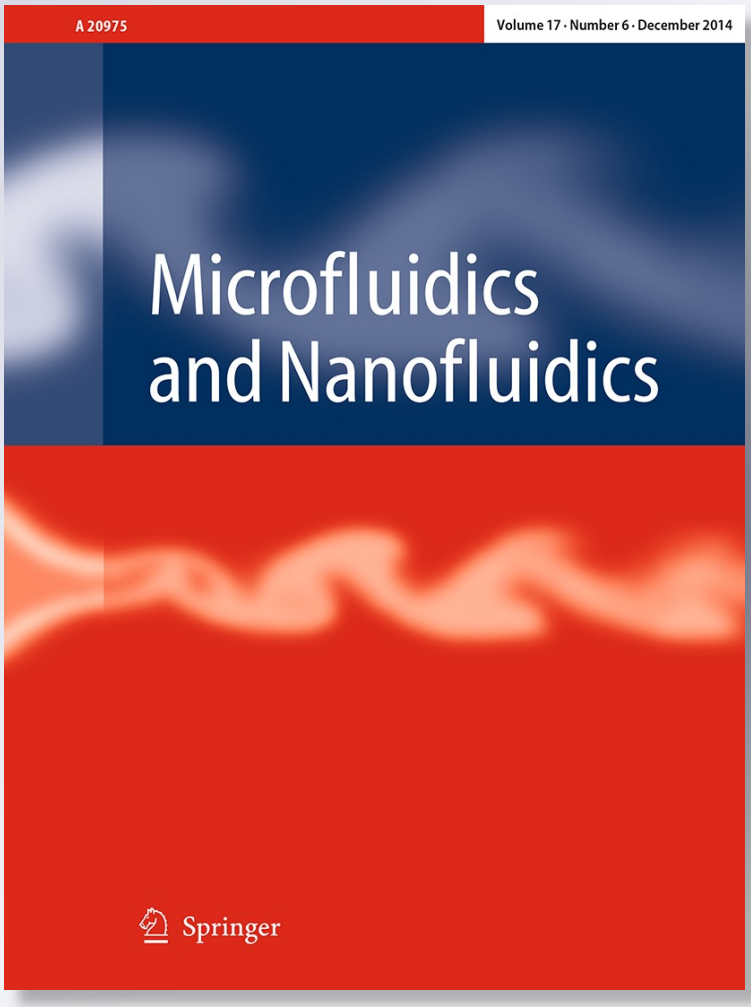

Springer

Microfluid Nanofluid (2014) 17:993–1002
DOI 10.1007/s10404-014-1392-0

RESEARCH PAPER

Electric field gradients during electrophoretic fractionation in microfabricated post arrays

Shokoufeh Kazemlou · Neda Nazemifard

Received: 24 September 2013 / Accepted: 23 March 2014 / Published online: 3 April 2014

Abstract Electrokinetic separation methods have been used extensively in microfluidic devices due to their separation power and compatibility with miniaturization platform. Electrophoresis (EP) fractionation of DNA and proteins in microfluidic devices has been conducted successfully and incorporated toward developing diagnostic devices. Porous structures as well as microfabricated pillars are often used as separation media for separation of biomolecules. The presence of the solid structures can create electric field gradients resulting in dielectrophoresis (DEP) which most often was neglected during DNA and protein fractionation. In this study, we evaluated the effect of induced field gradients by calculating the magnitude of the three most occurring phenomena during electrophoretic fractionation of biomolecules, i.e., EP, Brownian diffusion, and DC DEP in uniformly patterned post arrays. A mathematical model of convection–diffusion–migration of these charged entities was developed and solved using finite element analysis. Non-dimensional parameters were defined as a measure to predict the particles transport mechanism within the microfabricated post arrays in the presence of field gradients caused by the posts. Based on the properties of particles and the medium, our numerical analysis provided criteria to predict when the DEP can significantly alter the fate of the charged entities through uniform post arrays and therefore cannot be neglected. In order to identify these criteria, a generalized approach based on a systematic parametric study of particle size and zeta potentials was conducted. The criteria obtained have the potential to shed light on some of the challenges such as irreversible trapping and large band broadening during fractionation of charged macromolecules.

Keywords Electrophoresis · Dielectrophoresis · Microfluidics · Transport phenomena · DNA trapping

S. Kazemlou · N. Nazemifard (✉)
Department of Chemical and Materials Engineering, University of Alberta, Rm. 7-060 ECERF Building, Edmonton, AB T6G 2V4, Canada
e-mail: nn1@ualberta.ca

S. Kazemlou
e-mail: kazemlou@ualberta.ca

1 Introduction

Separation and fractionation of macromolecules such DNA, RNA, and proteins is one of the primary steps in any genetic analysis. The growing trend in developing high-speed hand-held diagnostic devices necessitates miniaturizing the conventional separation devices which has been the driving force for the recent advancement of microfluidics (Easley et al. 2006; Kourkine et al. 2002; Liu et al. 2006; Liu and Mathies 2009; Marcy et al. 2007; Mastrangelo et al. 1998; Pal et al. 2005; Zeng et al. 2010). The combined advantages of microfluidic platforms and electrokinetic phenomena resulted in micro scale devices capable of fractionating large molecules in a few seconds (Salieb-Beugelaar et al. 2009; Zeng et al. 2008; Bakajin et al. 2001; Liu and Mathies 2009). Microfabricated post arrays (MFPAs) are often used as the separation matrix due to the exact control in defining the post size, arrangements, and distances. In the majority of electrophoretic fractionation involving MFPA, the surface of the posts and the microchannel walls was modified to bear zero surface charges in order to negate the electroosmosis velocity of the medium which is in the opposite direction of the electrophoretic velocity of the molecules and can suppress the separation efficiency of the microchip significantly

(Ghosal 2004; Llopis et al. 2007; Slater et al. 2010). As a result, the two most dominant mechanisms for transport of charged macromolecules through MFPA under the externally applied electric fields are stated to be electrophoresis (EP) and Brownian diffusion (Minc et al. 2005; Viovy 2000; Shendruk et al. 2012; Slater et al. 2009). Although the two mentioned mechanisms are capable of explaining and predicting the configurations and the mobilities of the macromolecules during electrophoretic fractionation, there are still complicated molecular behaviors which cannot be explained by the two mechanisms. One is the irreversible entanglement of large DNA and RNA molecules around the posts under strong electric fields which poses a significant limitation on the size of DNA and RNA molecules resolved by microfluidic techniques (Akerman 1997; Bustamante et al. 1993; Duke 1993; Duke et al. 1996; Gurrieri et al. 1999; Ueda et al. 1998; Viovy et al. 1992a, b; Volkmuth et al. 1995; Sheng and Harrison 2013). The other is the relatively large band broadening (even when all the known sources of band broadening has been accounted for) during electrophoretic separation of biomolecules in porous structures which reduces the separation efficiency of the device (Ghosal 2004; Meistermann and Tinland 1998; Mercier and Slater 2006). In this study, in addition to the two mentioned transport mechanisms (EP and Brownian diffusion), the transport of charged particles in the presence of dielectrophoresis (DEP) effects in a MFPA is evaluated. Several criteria were defined based on physical and dielectric properties of the particle and medium, where the effects of DEP are significant and cannot be overlooked.

Particles subjected to spatially non-uniform electric fields experience electrical forces that can cause both EP and DEP. Electrophoretic forces are well chronicled and generally result from the hydrodynamic frictional forces balancing electrostatic forces (Hunter 2000). For the DEP, the translational force can cause motion toward increasing local field strength (positive DEP) or decreasing field strength (negative DEP) (Morgan and Green 2002). One common way of creating DEP is called DC DEP (or insulator-based DEP) where the voltage is applied by the two electrodes across a post array structure (Lapizco-Encinas et al. 2004a, b; Regtmeier et al. 2007, 2010). The presence of the post structures creates regions of higher and lower field strengths, resulting in the non-uniform electric fields necessary for DEP to occur.

In this manuscript, we evaluated the relative magnitude of DC DEP and EP and its influence on concentration of particles through uniformly patterned arrays of posts. Our objective was to mimic the experimental conditions common during electrophoretic fractionation of biomolecules to identify the operating conditions under which DEP particle trapping in the vicinity of the posts occurs and cannot be ignored. Changing the parameters affecting the response of the particles to the applied electric field, such as zeta potential of the particles, medium permittivity and particle size can change the relative magnitude of EP with respect to DEP. The geometry studied in this work (shown in Fig. 1) is also a typical design of microfluidic channel including arrays of micro scale posts that have been used in several studies for DNA and protein fractionation. A suspending solution is introduced into the channel, and a DC voltage is applied to electrodes located in inlet and outlet reservoirs. Upon applying the electric field, the field non-uniformities are generated due to the presence of post arrays inside the microchannel. The magnitude of induced field gradients depends on the ratio of post-to-post distance to post diameter, post shape, and arrangement (Dorfman 2010; Kazemlou and Nazemifard 2012). EP is used to transport the particles through the channel. As the particles are migrating through the post array, they are concentrated according to their characteristic physical and dielectric properties in response to electrophoretic, dielectrophoretic, and Brownian forces. Particle concentration profiles were calculated by solving the convection–diffusion–migration (CDM) equation of particles under EP, DEP, and Brownian forces using a finite element scheme. The objective was to define non-dimensional parameters based on the physical properties of particles and the medium to characterize the governing mechanism of particle transport through post arrays in the presence of field heterogeneities.

It is worth mentioning here that in this study, the effects of Joule heating have been neglected due to the relatively small electric field involved during the separation of charged molecules. The Joule heating effects cannot be ignored during DC DEP applications where extremely high electric fields are applied to manipulate cells and uncharged entities (Hawkins and Kirby 2010; Erickson et al. 2003).

2 Theory

The transport of particles in a microchannel filled with conductive media through an array of micro scale posts is governed by the general mass conservation equation (all the vector quantities are in bold) (Masliyah and Bhattacharjee 2006)

$$\frac{\partial c}{\partial t} = -\nabla \cdot \boldsymbol{j} + R \tag{1}$$

where c is the scaled particle concentration, $\boldsymbol{j}$ is the particle flux, and R is the rate of production due to chemical reaction per unit volume. For a dilute particle suspension where particle–particle interaction can be safely neglected, $\boldsymbol{j}$ consists of flux due to convection, diffusion, and migration under the influence of external forces

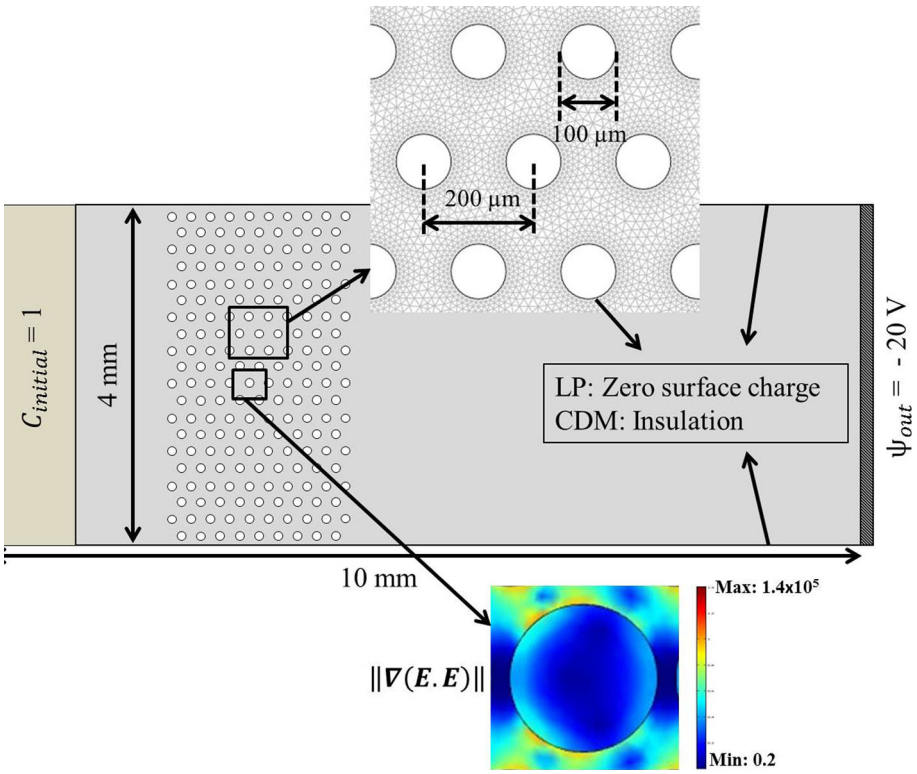

Fig. 1 Schematic of the geometry solved in our simulations illustrating the dimensions, initial condition, and boundary conditions. It consists of a microchannel 10 mm long, 4 mm wide and 10 μm deep, containing an array of 10 columns × 20 rows of posts 100 μm in diameter and arranged 200 μm center to center. Zero surface charge condition (for the Laplace equation) and insulation condition (for the CDM equation) are applied to the posts and the interior surface of the microchannel. A sample of 1 mM of particle solution was introduced at the inlet reservoir, and electrodes placed at the reservoirs applied electric potential of 40 V across the microchannel. The *top inset* shows the mesh configuration where higher mesh densities were used around the posts for accurate calculations of electric field gradients. The *bottom inset* shows the electric field gradient, $\|\nabla(E \cdot E)\|$ around the post in the middle of the microfabricated post array

$$\boldsymbol{j} = c\boldsymbol{u} - D\nabla c + \frac{cD}{k_{\mathrm{b}}T}\boldsymbol{F} \tag{2}$$

where $\boldsymbol{u}$ is the fluid velocity, D is the particle diffusion coefficient, k_{b} is the Boltzmann constant, T is the absolute temperature, and $\boldsymbol{F}$ is the total force exerted on the particles. In the absence of any chemical reaction ($R = 0$) in the stationary fluid flow ($u = 0$), substituting $\boldsymbol{j}$ in Eq. 1 by its definition from Eq. 2, the CDM equation of the particles can be written as:

$$\frac{\partial c}{\partial t} + \nabla \cdot \left(c\frac{D}{k_b T}\boldsymbol{F} - D\nabla \mathrm{c} \right) = 0 \tag{3}$$

The diffusion coefficient can be obtained from the following equation:

$$D = \frac{k_{\mathrm{b}}T}{6\pi\mu r} \tag{4}$$

where μ is the viscosity of the electrolyte solution and r is the particle radius. A suspended particle subjected to a spatially non-uniform electric field experiences electrical forces that can cause both EP and DEP. The total electrical force ($\boldsymbol{F}$) exerted on a particle can be calculated by the sum of the electrophoretic and dielectrophoretic forces it experiences

$$\boldsymbol{F} = \boldsymbol{F}_{\mathrm{EP}} + \boldsymbol{F}_{\mathrm{DEP}} \tag{5}$$

For a spherical particle of radius r, in a high concentration electrolyte solution, when the Debye screening layer is small relative to the particle radius, i.e., $\kappa r \gg 1$, the electrophoretic force can be obtained from the following equation (Masliyah and Bhattacharjee 2006)

$$\boldsymbol{F}_{\mathrm{EP}} = 6\pi r\varepsilon_r\varepsilon_0\zeta\boldsymbol{E} \tag{6}$$

where ε_r is the relative permittivity of the medium, ε_0 is the permittivity of free space, ζ is the zeta potential at the particle surface, and $\boldsymbol{E}$ is the externally applied electric field. Dielectrophoretic force exerted on a spherical particle in a non-uniform electric field is given by (Morgan and Green 2002)

$$\boldsymbol{F}_{\mathrm{DEP}} = \pi\varepsilon_r\varepsilon_0 r^3 Re[f_{\mathrm{CM}}]\nabla(\boldsymbol{E}\cdot\boldsymbol{E}) \quad (7)$$

where $Re[f_{\mathrm{CM}}]$ is the real part of the Clausius–Mossotti factor. In the low frequency or DC limit, the Clausius–Mossotti factor (consequently polarization) depends solely on the conductivity of the particle and suspending medium and can be approximated by (Morgan and Green 2002)

$$f_{\mathrm{CM}} = \frac{\sigma_{\mathrm{p}} - \sigma_{\mathrm{m}}}{\sigma_{\mathrm{p}} + 2\sigma_{\mathrm{m}}} \quad (8)$$

where σ_{p} and σ_{m} are the real conductivities of the particle and medium, respectively. Positive DEP (movement toward strong field region) occurs when a particle is more polarizable than the medium $(\sigma_{\mathrm{p}} > \sigma_{\mathrm{m}})$,, whereas negative DEP (movement away from strong field region) occurs if a particle is less polarizable $(\sigma_{\mathrm{p}} < \sigma_{\mathrm{m}})$. The particles considered in this study have higher conductivities than the medium and experience positive DEP.

3 Numerical simulation

Finite element method is one of the most commonly used methods of solving a system of partial differential equations including the mass transfer equations in literature (Hu et al. 2003; Cordovez et al. 2007; Thormann et al. 2010). We used the finite element method to solve the CDM equation of the particles (Eq. 3) in the two-dimensional geometry as shown in Fig. 1. The numerical simulation is conducted using commercially available software, COMSOL Multiphysics. The local value of electric field, E, in our geometry was calculated by solving the Laplace (LA) equation $(\nabla^2\psi = 0)$ with the following boundary conditions:

$$\boldsymbol{n}\cdot\boldsymbol{I} = 0 \text{ at the microchannel boundaries and around the posts} \quad (9a)$$

$$\psi = \psi_{\mathrm{in}} \text{ at channel inlet} \quad (9b)$$

$$\psi = \psi_{\mathrm{out}} \text{ at channel outlet} \quad (9c)$$

where ψ is the electric potential, $\boldsymbol{n}$ is the normal vector to the surface, $\boldsymbol{I}$ is the electrical current, and $\psi_{\mathrm{in}} - \psi_{\mathrm{out}}$ is the electrical potential applied between the electrodes. From the solution of LA equation, numerical values for the electric field and electric field gradients were obtained in the post array geometry. Using the local values of electric field and field gradients, the electrophoretic and dielectrophoretic forces can be calculated using Eqs. 6 and 7, respectively.

Figure 1 illustrates the geometry of the two-dimensional microchannel studied in our simulations. It consists of a microchannel 10 mm long, 4 mm wide, and 10 μm deep, containing an array of 10 columns × 20 rows of posts 100 μm in diameter and arranged 200 μm center to center. Hexagonal arrangement and circular cross-sectional posts were considered for the post array. A sample of 1 mM of particle solution was introduced at the inlet reservoir, and electrodes placed at the reservoirs applied electric potential of 40 V across the microchannel.

The initial and boundary conditions employed in the simulations in order to solve the LA, and CDM equation are presented in Fig. 1. A triangular mesh configuration was used to discretize the geometry in order to solve both LA and CDM equations. Instead of a uniform mesh configuration, a more refined mesh configuration was used in the vicinity of the posts, sharp corners, and along the intersection with the ratio of the mesh density around the posts to the mesh density in the bulk of ten as shown in the inset of Fig. 1 to ensure the accuracy of the calculation. Finite element analysis was applied in a triangular mesh of around 400,000 elements and 200,000 nodal points. It was observed that such a refined mesh configuration was sufficient to provide electric field values independent of the number of elements.

It is worth mentioning here that the range of the parameters employed in our simulations (Table 1) is chosen to be similar to the experimental parameters during electrophoretic fractionation of biomolecules such as DNA and proteins. The applied electric fields during most of DNA and protein EP are around 10–100 V/cm. The medium permittivity values were chosen to accommodate a wide selection of solvents ranging from organic solvents to common DNA electrophoresis solvents such as TBE. The particle sizes were from a few nanometers to a few micrometers to represent both charged molecules and charged macromolecules such as DNA which can be modeled as sphere-spring chains. A dilute suspension of particles were considered, so the particle–particle interaction can be neglected.

Table 1 The ranges of parameters used in the simulation

Parameter	Value	Unit
Voltage applied on the inlet electrode, ψ_{in}	20	V
Voltage applied on the outlet electrode, ψ_{out}	−20	V
Diameter of the posts, d	(50–200)	μm
Spacing between the posts, a	(50–200)	μm
Particle radius, r	(0.01–5)	μm
Zeta potential of the particle, ζ	(0.01–100)	mV
Medium relative permittivity, ε_{r}	(5–70)	–
Conductivity of the medium, σ_{m}	5.5×10^{-5}	S/m
Conductivity of the particle, σ_{p}	7.5×10^{-5}	S/m

4 Results and discussion

The exact solution of local electric field in post array structure coupled with CDM equation has been used to define the migration mechanism of particles through MFPA geometry. Using the finite element method, it was possible to conduct a systematic parametric study to define a range of parameters affecting the response of the particles to the applied electric field, such as particle size, permittivity of the medium, and zeta potential of the particles. The inset in Fig. 1 shows the surface plot of the numerically calculated electric field gradient around the middle post in our geometry. A comprehensive study on the electric field and its gradient and how they are affected by the geometry and arrangement of the posts in MFPA has been published by the authors elsewhere (Kazemlou and Nazemifard 2012).

In order to emphasize the importance of considering all the migration mechanisms during electrophoretic migration of charged entities in a stationary medium through MFPA geometry, two scenarios were considered and shown in Fig. 2. Figure 2a, b show the particle concentration profile in the post arrays section of the microchannel while Fig. 2c, d present the particle concentration profile in the detection section once the particles passed through the post array. In what follows, the detection section, where concentration profiles were calculated, assumed to be at the distance of 1.5 mm from the end of the post array. Figure 2a, c are obtained with the assumption that the only external force on the particles is EP ($F_{DEP} = 0$), while Fig. 2b, d are obtained with the assumption that the external forces on the particles are EP and DEP ($F_{DEP} \neq 0$). Although the relative magnitude of DEP force to EP force here is very small (around 0.01), one can observe that the concentration profile and the maximum particle concentration have been significantly influenced by the presence of the DEP. This implies the importance of considering DEP as a defining transport mechanism that can change the fate of particles especially those with trajectories in the vicinity of the posts.

In mass transfer literature, the relative role of the contributions from convection and diffusion is usually determined by the value of the so-called Peclet number $Pe = rU/D$, where r is the particle radius, U is the relative velocity of a particle with respect to the liquid, and D is the

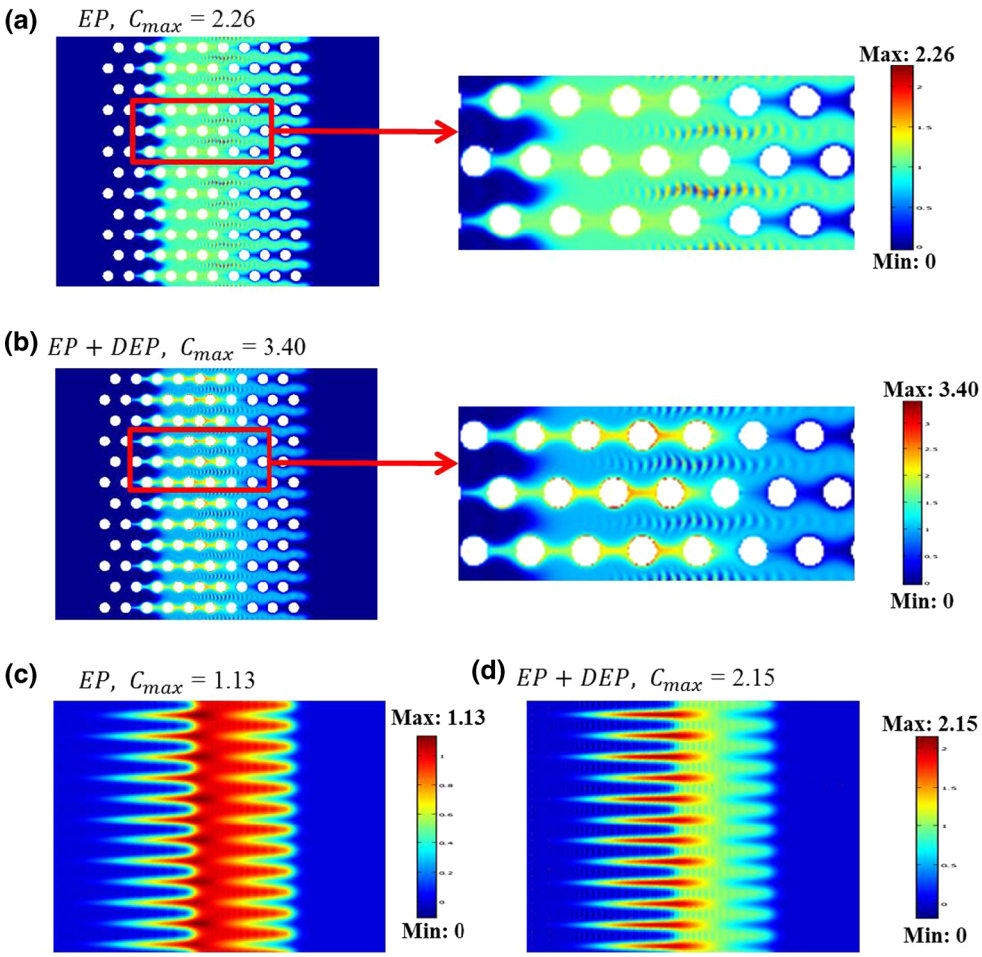

Fig. 2 Schematic illustrates the effect of DEP on configuration of particles concentration profile. The relative magnitude of DEP to EP forces is around 0.01 and the particle size, medium permittivity and zeta potential of the particles are $r = 5$ μm, $\varepsilon_r = 1$, and $\zeta = 1$ mV. **a**, **b** Show the concentration profile, while particles are passing through the posts **a** ignoring DEP effect, **b** considering DEP. **c**, **d** Present the configuration of the concentration profile after passing the post array **c** ignoring DEP, **d** considering DEP. The significant change in the concentration profile, due to adding DEP effect, reveals the necessity of considering DEP as an effective mechanism in particles transport within the microfabricated devices

diffusion coefficient of the particle (Bird et al. 2006). As described earlier, charged particles subjected to a non-uniform electric field experience dielectrophoretic forces in addition to electrophoretic forces. To define the relative effects of these two forces, simulations were conducted to obtain the operating conditions, in form of particle and medium properties, under which the dielectrophoretic forces play a major role in changing the particles trajectories. The results are presented as variation of the relative value of the Peclet numbers associated with EP and DEP velocities, Pe_{EP}/Pe_{DEP} calculated based on different particle and medium properties. Pe_{EP} and Pe_{DEP} were calculated using $Pe_{EP} = rU_{EP}/D$ and $Pe_{DEP} = rU_{DEP}/D$. U_{EP} and U_{DEP} are the maximum electrophoretic and dielectrophoretic particle velocities and are defined as $U_{EP} = F_{EP}/6\pi\mu r$ and $U_{DEP} = F_{DEP}/6\pi\mu r$ where F_{EP} and F_{DEP} were calculated by solving the LA equation ($\nabla^2\psi = 0$) of electric field numerically and substituting the calculated values of E and $\Delta(E{\cdot}E)$ in Eqs. 6 and 7.

Although the presence of DEP forces can change the particle trajectory in the vicinity of the posts, as long as the particle trajectory does not intersect with the post surface, no irreversible trapping of particles around the posts occur. We used this observation to quantify the relative effects of EP and DEP on particle fate through MFPA under the applied electric field as shown in the schematic in Fig. 3. The irreversible trapping happens when DEP forces on particles in the vicinity of the posts are strong enough to push the particles toward the post surface until the surface-to-surface distance is close to zero. Using the particle concentration profiles and an integration scheme, one can calculate the total number of the particles at the inlet and the detection section after the post array. The comparison of the particle numbers before and after the post arrays shows how many particles are trapped irreversibly around the posts due to DEP forces. Throughout this study, we assumed the effect of DEP is significant once 10 % of the inlet particles are trapped inside the MFPA.

The particle concentration profiles were calculated as described in "Numerical simulation" section for different particle sizes, particle zeta potentials, and relative permittivity of the media. It was observed that when the value of $Pe_{DEP}/Pe_{EP} = 0.03 \pm 0.006$, 10 % of the inlet particles are trapped around the posts due to the presence of high field gradients in the vicinity of the posts meaning, the effects of DEP are significant and cannot be neglected. The simulations were conducted for three different post array geometries with post diameters and post-to-post distances shown in Table 1. For all these geometries, it was observed that around the same ratio of $Pe_{DEP}/Pe_{EP} \approx 0.03$, tenth of the feed particles are trapped inside MFPA regardless of the post size and arrangement. We calculated the ratio of Pe_{DEP}/Pe_{EP} with respect to particle size and particle zeta potential to associate this ratio to the physical properties of the charged entities. The results have been shown in Fig. 4a, b. It can be seen from these two figures that $Pe_{DEP}/Pe_{EP} \approx 0.03$ can be associated with electrophoretic motion of particle with radius of 1 μm and zeta potential of 10 mV.

To further quantify the effect of DEP on separation efficiency during electrophoretic motion of charged entities

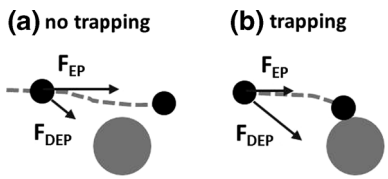

Fig. 3 Schematic a charged particle trajectory in the vicinity of a post where **a** DEP forces bring the particles close to the posts but no trapping occurs and **b** DEP forces are strong enough to bring the charged particle to the surface of the posts when the trapping occurs. *Dashed lines* are particle trajectory

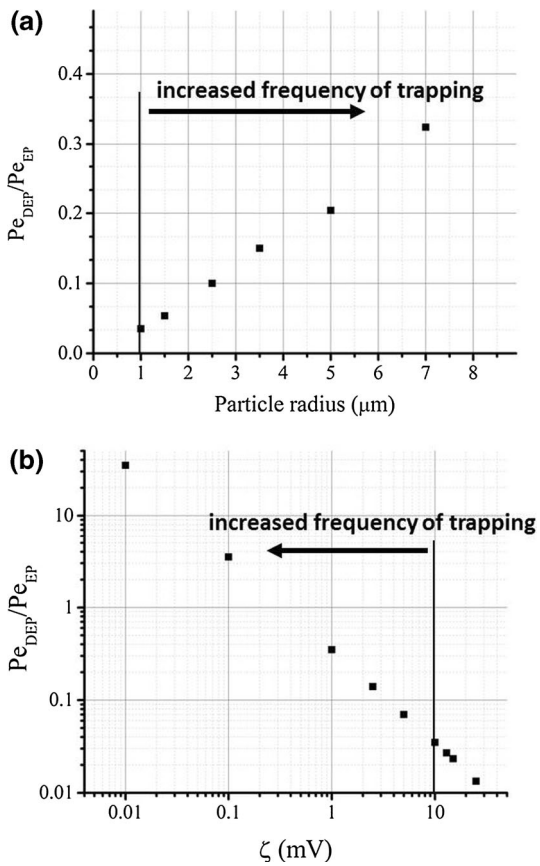

Fig. 4 Variation of Pe_{DEP}/Pe_{EP} with respect to **a** particle radius and **b** particle zeta potential. It was observed for Pe_{DEP}/Pe_{EP} around 0.03 tenth of feed particles are trapped around the posts permanently; this ration corresponds to particle radius of around 1 μm with zeta potential of 10 mV

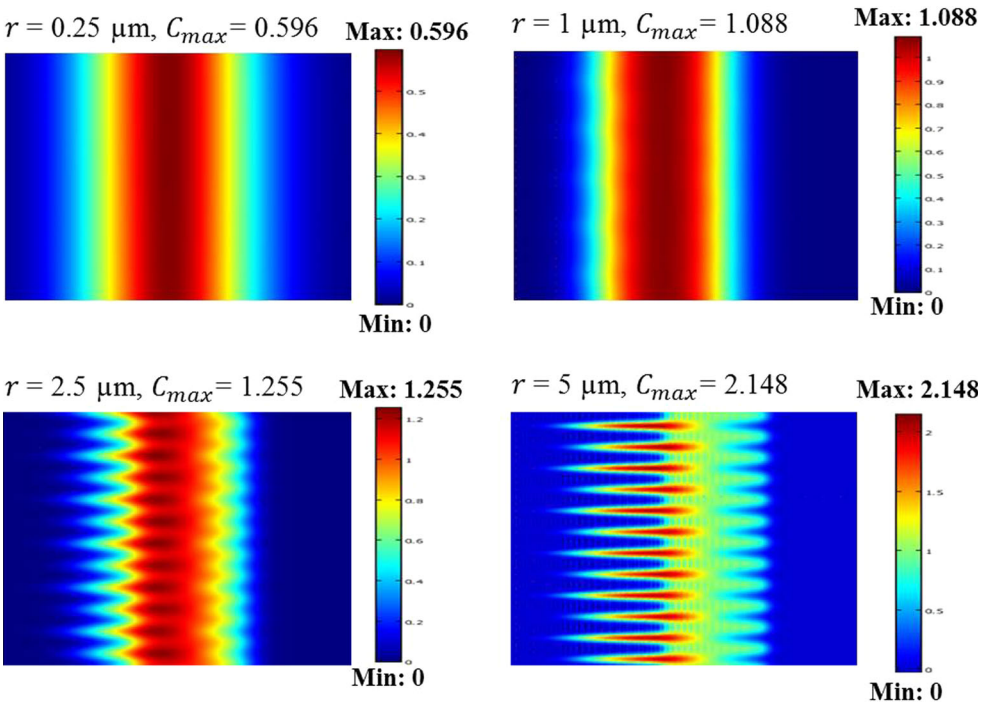

Fig. 5 Schematic illustration of concentration profile configuration for different particle sizes after passing through the post array. By increasing the particle size, and consequently the Pe_{DEP}/Pe_{EP} ratio, the concentration profile renders to discrete and more concentrated regions

through MFPA, we calculated the band broadening of the concentration profiles once the particles pass through the post arrays. For a normal distribution, the band broadening is usually measured by the standard deviation. Since the concentration profiles obtained in this study were not normally distributed, the semi interquartile range which is often used with skewed data was employed instead of standard deviation to measure the band broadening.

The influence of particle size and zeta potential on particle concentration profile as well as band broadening is shown in Figs. 5, 6, 7, and 8.

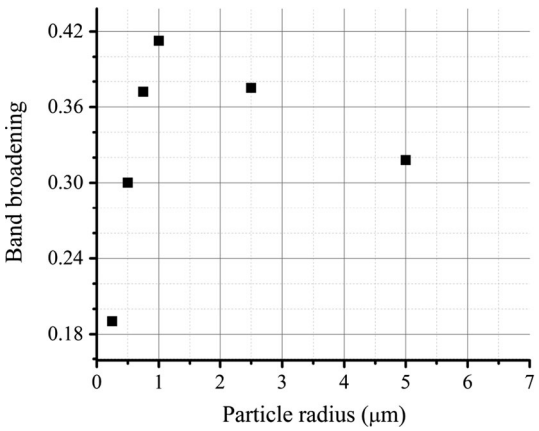

Fig. 6 Relation between the band broadening and particle size based on our simulation results. Increasing the particle size, the band broadening increases first, reaches its maximum value at particle radius of 1 μm, and then decreases

4.1 Particle size

Figure 5 illustrates concentration profile for different particle sizes after passing through the post array. The same post array as Fig. 1 was used in the simulations here. All parameters, apart from particle size, were kept constant. Zeta potential of 1 mV and medium permittivity of 70 were used. According to Fig. 5, as the particle size increased the concentration profile has been changed from a uniform configuration to discrete regions due to the presence of high dielectrophoretic forces. Furthermore, increasing the particle size (higher relative values of DEP force to EP force) results in more concentrated profiles with higher values of maximum concentration, C_{max}, in each profile. The influence of particle size on band broadening of the concentration profile was presented in Fig. 6. The effect of particle size on band broadening originates from the interplay of diffusion forces, EP, and DEP forces and how their values are affected by the particle size. Higher diffusion results in higher band broadening and diffusion are higher for smaller particles (Eq. 4). On the other hand, higher DEP results in higher band broadening in array geometry (since it disturbs the uniform velocity of the particles, those closer to the posts will be slowed down compared to the particles away from the posts) and DEP is higher for larger particles (Eq. 7). That is why most of the numerical as well as experimental studies on the variation of band broadening with particle size show a non-monotonous variation. Our results in Fig. 6 show that by increasing the particle size, the band broadening increases

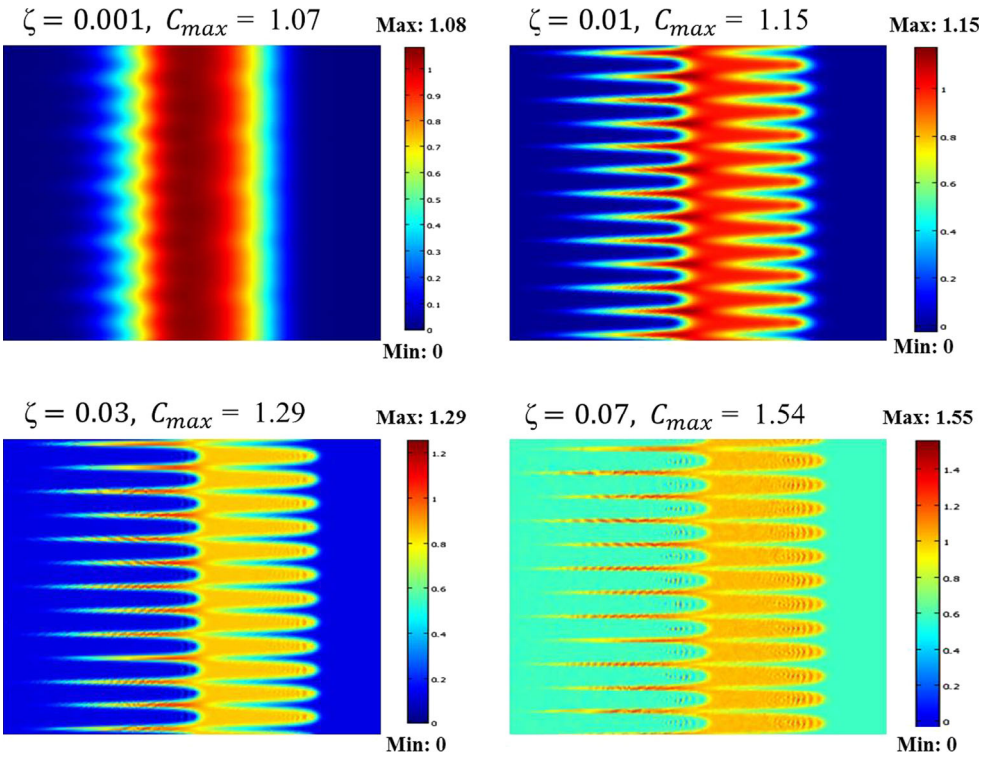

Fig. 7 Schematic illustration of the concentration profile after the particles pass the post array for different values of zeta potential. Increasing the zeta potential, and consequently the relative magnitude of electrophoresis to diffusion, provides higher maximum concentrations. However, these profiles are not as concentrated as the profiles obtained by increasing the Pe_{DEP}/Pe_{EP} ratio (Fig. 5)

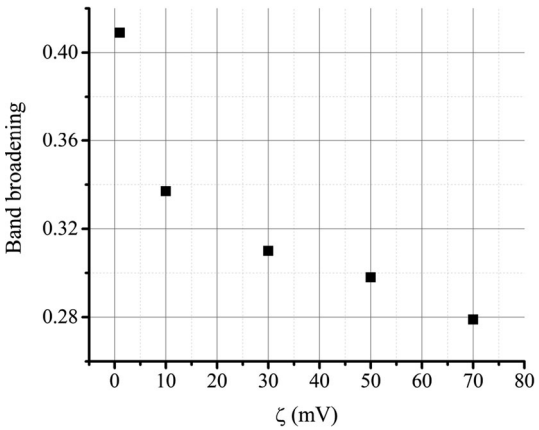

Fig. 8 Variation of the band broadening of the concentration profile with respect to zeta potential of the particles. Increasing the zeta potential increases the relative magnitude of the electrophoresis to diffusion, which results in less band broadening of the concentration profile

first (higher DEP), reaches its maximum value at particle radius of 1 μm, and then decreases (smaller diffusion), following the common trend shown in the literature.

4.2 Particle zeta potential

Calculations were made to investigate the effect of zeta potential of the particles on the concentration profile as shown in Fig. 7. The same geometry shown in Fig. 1 was used, and the values of particle size and relative medium permittivity of 0.5 μm and 70 were considered, respectively. As Fig. 7 shows, the concentration profile has been changed by increasing the zeta potential. However, this increase is not significant, which implies that by increasing the zeta potential, and consequently the relative magnitude of EP to diffusion, particles have less time to be dispersed due to diffusion which tends to homogenize the concentration profile, therefor the concentration profile becomes less uniform. Figure 8 plots the variation of band broadening of the concentration profile with respect to zeta potential of the particles. As this figure shows, the band broadening was decreased by increasing the zeta potential. The role of diffusion in increasing the band broadening is well known, however, the significance of this graph is in showing that DEP similar to diffusion tends to increase the band broadening during electrophoretic separation. At high zeta potentials, where the EP becomes the dominant force in defining the particle transport through the separation matrix, the influence of DEP and Brownian diffusion diminishes which results in smaller band broadening.

5 Conclusion

During electrophoretic separation of charged macromolecules, a rather complicated scenario can occur when porous structures or post arrays are used as sieving media which is a

common practice for in-chip separation of DNA and proteins. In the majority of these practices, the effect of DEP has been completely overlooked. Some of the unexplained phenomena observed during these experiments such as DNA trapping during DNA electrophoresis or high values of band broadening can be explained by taking into account the effects of DEP. As discussed earlier, the post array structures have been used extensively to create insulator-based DEP which shows their potential to create high electric field gradients and non-negligible DEP forces. This necessitates defining criteria at which the DEP effects are insignificant and can be safely ignored compared with other transport mechanism involved in post arrays structure. Defining these criteria has been the objective of this manuscript. In this study, the fate of charged particles through uniform arrays of posts was studied in the presence of diffusion, EP, and DEP forces. Using finite element methods, we introduced criteria based on the particles and medium properties and magnitude of the applied field, where DEP forces have significant effects on particles trajectories during electrophoretic migration through MFPA. The results were presented in form of Peclet numbers which show the relative role of the contributions from electrophoretic and dielectrophoretic induced convection with respect to diffusion. It was observed that there is a critical value for the relative magnitude of the electrophoretic and dielectrophoretic forces, in form of Pe_{DEP}/Pe_{EP}, above which the DEP has the potential to trap particles around the posts permanently. Different post arrays with different post sizes and post-to-post distances were studied, and it was observed that around this critical value the particle trapping occurs independent of MFPA geometry. Further simulations were conducted to understand the influence of the particle size and zeta potential on the particles concentration profile and band broadening. It was observed that by increasing the particle size, and consequently the relative magnitude of Pe_{DEP}/Pe_{EP}, the configuration of the concentration profile rendered to some discrete and more concentrated regions which resulted in higher band broadenings.

Our observations show the increase in band broadening and the number of trapped particles can be captured in the mass transfer model once the effects of DEP is included. Although compared with insulator-based DEP, the values of electric fields applied during electrophoretic separation of charged molecules are orders of magnitude smaller, but due to the presence of solid post arrays and the micro scales post-to-post distances, DEP effects can still be nontrivial. Since DNA molecules have been commonly modeled using bead-spring chains, our preliminary results for particle transport can be improved to discover the extend of DEP contribution in DNA trapping during DNA electrophoresis which is one of biggest hurdles in achieving high-speed high-efficiency DNA fractionation.

Acknowledgments The authors thank financial support from Natural Sciences and Engineering Research Council of Canada (NSERC). We also thank nanoBridge at University of Alberta for providing the software for the numerical simulation.

References

Akerman B (1997) Threading dynamics of a polymer through parallel pores: potential applications to DNA size separation. J Chem Phys 106(14):6152–6159

Bakajin O, Duke TAJ, Tegenfeldt J, Chou CF, Chan SS, Austin RH, Cox EC (2001) Separation of 100-kilobase DNA molecules in 10 seconds. Anal Chem 73(24):6053–6056. doi:10.1021/ac015527o

Bird RB, Stewart WES, Lightfoot EN (eds) (2006) Transport phenomena, 2nd edn. Wiley, New York

Bustamante C, Gurrieri S, Smith SB (1993) Towards a molecular description of pulsed-field gel-electrophoresis. Trends Biotechnol 11(1):23–30. doi:10.1016/0167-7799(93)90071-g

Cordovez B, Psaltis D, Erickson D (2007) Trapping and storage of particles in electroactive microwells. Appl Phys Lett 90(2):024102. doi:10.1063/1.2430775

Dorfman KD (2010) DNA electrophoresis in microfabricated devices. Rev Mod Phys 82(4):2903–2947. doi:10.1103/RevModPhys.82.2903

Duke T (1993) Molecular mechanisms of DNA electrophoresis. Int J Genome Res 1(3):227–247

Duke TAJ, Austin RH, Cox EC, Chan SS (1996) Pulsed-field electrophoresis in microlithographic arrays. Electrophoresis 17(6):1075–1079. doi:10.1002/elps.1150170616

Easley CJ, Karlinsey JM, Bienvenue JM, Legendre LA, Roper MG, Feldman SH, Hughes MA, Hewlett EL, Merkel TJ, Ferrance JP, Landers JP (2006) A fully integrated microfluidic genetic analysis system with sample-in-answer-out capability. Proc Natl Acad Sci USA 103(51):19272–19277. doi:10.1073/pnas.0604663103

Erickson D, Sinton D, Li DQ (2003) Joule heating and heat transfer in poly (dimethylsiloxane) microfluidic systems. Lab Chip 3(3):141–149. doi:10.1039/b306158b

Ghosal S (2004) Fluid mechanics of electroosmotic flow and its effect on band broadening in capillary electrophoresis. Electrophoresis 25(2):214–228. doi:10.1002/elps.200305745

Gurrieri S, Smith SB, Bustamante C (1999) Trapping of megabase-sized DNA molecules during agarose gel electrophoresis. Proc Natl Acad Sci USA 96(2):453–458. doi:10.1073/pnas.96.2.453

Hawkins BG, Kirby BJ (2010) Electrothermal flow effects in insulating (electrodeless) dielectrophoresis systems. Electrophoresis 31(22):3622–3633. doi:10.1002/elps.201000429

Hu YD, Werner C, Li DQ (2003) Electrokinetic transport through rough microchannels. Anal Chem 75(21):5747–5758. doi:10.1021/ac0347157

Hunter RJ (2000) Foundations of colloid science. Oxford University Press, New York

Kazemlou S, Nazemifard N (2012) Electric field gradients in micro/nanofluidic devices. In: ASME international mechanical engineering and exposition. Houston, TX, pp 339–346

Kourkine IV, Hestekin CN, Buchholz BA, Barron AE (2002) High-throughput, high-sensitivity genetic mutation detection by tandem single-strand conformation polymorphism/heteroduplex analysis capillary array electrophoresis. Anal Chem 74(11):2565–2572. doi:10.1021/ac020025b

Lapizco-Encinas BH, Simmons BA, Cummings EB, Fintschenko Y (2004a) Dielectrophoretic concentration and separation of live and dead bacteria in an array of insulators. Anal Chem 76(6):1571–1579. doi:10.1021/ac034804j

Lapizco-Encinas BH, Simmons BA, Cummings EB, Fintschenko Y (2004b) Insulator-based dielectrophoresis for the selective concentration and separation of live bacteria in water. Electrophoresis 25(10–11):1695–1704. doi:10.1002/elps.200405899

Liu P, Mathies RA (2009) Integrated microfluidic systems for high-performance genetic analysis. Trends Biotechnol 27(10): 572–581. doi:10.1016/j.tibtech.2009.07.002

Liu CN, Toriello NM, Mathies RA (2006) Multichannel PCR-CE microdevice for genetic analysis. Anal Chem 78(15):5474–5479. doi:10.1021/ac060335k

Llopis SL, Osiri J, Soper SA (2007) Surface modification of poly(methyl methacrylate) microfluidic devices for high-resolution separations of single-stranded DNA. Electrophoresis 28(6):984–993. doi:10.1002/elps.200600435

Marcy Y, Ouverney C, Bik EM, Losekann T, Ivanova N, Martin HG, Szeto E, Platt D, Hugenholtz P, Relman DA, Quake SR (2007) Dissecting biological "dark matter" with single-cell genetic analysis of rare and uncultivated TM7 microbes from the human mouth. Proc Natl Acad Sci USA 104(29):11889–11894. doi:10.1073/pnas.0704662104

Masliyah JH, Bhattacharjee S (eds) (2006) Electrokinetic and colloid transport phenomena, 1st edn. Wiley-Interscience, New York

Mastrangelo CH, Burns MA, Burke DT (1998) Microfabricated devices for genetic diagnostics. Proc IEEE 86(8):1769–1787. doi:10.1109/5.704282

Meistermann L, Tinland B (1998) Band broadening in gel electrophoresis of DNA: measurements of longitudinal and transverse dispersion coefficients. Phys Rev E 58(4):4801–4806. doi:10.1103/PhysRevE.58.4801

Mercier JF, Slater GW (2006) Universal interpolating function for the dispersion coefficient of DNA fragments in sieving matrices. Electrophoresis 27(8):1453–1461. doi:10.1002/elps.200500532

Minc N, Viovy JL, Dorfman KD (2005) Non-Markovian transport of DNA in microfluidic post arrays. Phys Rev Lett 94(19):198105. doi:10.1103/PhysRevLett.94.198105

Morgan H, Green NG (ed) (2002) AC electrokinetics: colloids and nanoparticles, 1st edn. Research Studies Press LTD, Hertfordshire

Pal R, Yang M, Lin R, Johnson BN, Srivastava N, Razzacki SZ, Chomistek KJ, Heldsinger DC, Haque RM, Ugaz VM, Thwar PK, Chen Z, Alfano K, Yim MB, Krishnan M, Fuller AO, Larson RG, Burke DT, Burns MA (2005) An integrated microfluidic device for influenza and other genetic analyses. Lab Chip 5(10):1024–1032. doi:10.1039/b505994a

Regtmeier J, Duong TT, Eichhorn R, Anselmetti D, Ros A (2007) Dielectrophoretic manipulation of DNA: separation and polarizability. Anal Chem 79(10):3925–3932. doi:10.1021/ac062431r

Regtmeier J, Eichhorn R, Bogunovic L, Ros A, Anselmetti D (2010) Dielectrophoretic trapping and polarizability of DNA: the role of spatial conformation. Anal Chem 82(17):7141–7149. doi:10.1021/ac1005475

Salieb-Beugelaar GB, Dorfman KD, van den Berg A, Eijkel JCT (2009) Electrophoretic separation of DNA in gels and nanostructures. Lab Chip 9(17):2508–2523. doi:10.1039/b905448k

Shendruk TN, Hickey OA, Slater GW, Harden JL (2012) Electrophoresis: when hydrodynamics matter. Curr Opin Colloid Interface Sci 17(2):74–82. doi:10.1016/j.cocis.2011.08.002

Sheng H, Harrison DJ (2013) Effect of intermittent and high field on trapping of megabase-sized DNA under asymmetric pulsed field in nanoporous structures on chip. MicroTAS 2013:1203–1205

Slater GW, Holm C, Chubynsky MV, de Haan HW, Dube A, Grass K, Hickey OA, Kingsburry C, Sean D, Shendruk TN, Nhan L (2009) Modeling the separation of macromolecules: a review of current computer simulation methods. Electrophoresis 30(5): 792–818. doi:10.1002/elps.200800673

Slater GW, Tessier F, Kopecka K (2010) The electroosmotic flow (EOF). In: Hughes MP, Hoettges KF (eds) Microengineering in biotechnology. Methods in molecular biology, vol 583., pp 121–134. doi:10.1007/978-1-60327-106-6_5

Thormann W, Breadmore MC, Caslavska J, Mosher RA (2010) Dynamic computer simulations of electrophoresis: a versatile research and teaching tool. Electrophoresis 31(5):726–754. doi:10.1002/elps.200900613

Ueda M, Oana H, Baba Y, Doi M, Yoshikawa K (1998) Electrophoresis of long DNA molecules in linear polyacrylamide solutions. Biophys Chem 71(2–3):113–123. doi:10.1016/s0301-4622(98)00093-3

Viovy JL (2000) Electrophoresis of DNA and other polyelectrolytes: physical mechanisms. Rev Mod Phys 72(3):813–872. doi:10.1103/RevModPhys.72.813

Viovy JL, Duke T, Caron F (1992a) The physics of DNA electrophoresis. Contemp Phys 33(1):25–40. doi:10.1080/00107519208219138

Viovy JL, Miomandre F, Miquel MC, Caron F, Sor F (1992b) Irreversible trapping of DNA during crossed-field gel-electrophoresis. Electrophoresis 13(1–2):1–6. doi:10.1002/elps.1150130102

Volkmuth WD, Duke T, Austin RH, Cox EC (1995) Trapping of branched DNA in microfabricated structures. Proc Natl Acad Sci USA 92(15):6887–6891. doi:10.1073/pnas.92.15.6887

Zeng Y, He M, Harrison DJ (2008) Microfluidic self-patterning of large-scale crystalline nanoarrays for high-throughput continuous DNA fractionation. Angew Chem Int Ed 47(34):6388–6391. doi:10.1002/anie.200800816

Zeng Y, Novak R, Shuga J, Smith MT, Mathies RA (2010) High-performance single cell genetic analysis using microfluidic emulsion generator arrays. Anal Chem 82(8):3183–3190. doi:10.1021/ac902683t